Contraction Diagram Analysis in Pion-Kaon Scattering

Chaitra Kalmahalli Guruswamy[a], Ulf-G. Meißner[a,b,c], Chien-Yeah Seng[a]

[a] *Helmholtz-Institut für Strahlen- und Kernphysik and Bethe Center for Theoretical Physics,*
Universität Bonn, D-53115 Bonn, Germany
[b] *Institute for Advanced Simulation, Institut für Kernphysik and Jülich Center for Hadron Physics,*
Forschungszentrum Jülich, D-52425 Jülich, Germany
[c] *Tbilisi State University, 0186 Tbilisi, Georgia*

Abstract

We study the contributions from the connected and disconnected contraction diagrams to the pion-kaon scattering amplitude within the framework of SU(4|1) partially-quenched chiral perturbation theory. Combining this with a finite-volume analysis, we demonstrate that a lattice calculation of the easier computable connected correlation functions is able to provide valuable information of the noisier disconnected correlation functions, and may serve as a theory guidance for the future refinement of the corresponding lattice techniques.

1. Introduction

Pion-kaon (πK) scattering is the simplest hadronic scattering process that involves a strange quark, and therefore it plays a crucial role in our understanding of the SU(3) chiral symmetry breaking of the Quantum Chromodynamics (QCD) [1]. The πK scattering amplitude was calculated within the framework of Chiral Perturbation Theory (ChPT) at one loop [2, 3] and at two loops [4], with the appearance of certain low-energy constants (LECs), some of which can be fixed in other processes. Naturally, this also provides motivation for the study of πK scattering using one of the standard first-principle treatments of the strong interaction, namely lattice QCD[1].

Furthermore, due to the similar isospin structures, an improved understanding of πK scattering also provides useful insights for πN scattering, which is an important ingredient towards resolving the current disagreement between the lattice [7, 8, 9, 10, 11] and the dispersion-theoretical [12, 13, 14, 15] determinations of the pion-nucleon sigma term.

So far there exists a number of exploratory studies of πK scattering, in both the $I = 3/2$ and $I = 1/2$ channels [16, 17, 18, 19, 20, 21, 22, 23]. The $I = 1/2$ channel is of much interest as it provides useful information about the K^* resonance, but it turns out that this channel is much more difficult to handle on the lattice, due to the existence of correlation functions involving the contraction of one or more pairs of quarks at the same temporal point (which are often called "disconnected diagrams"). Such diagrams have low signal-to-noise ratio, and are also the main reason for the increased difficulty in the lattice study of $\pi\pi$ scattering at lower isospin. Obviously, one cannot claim to have a controlled error analysis in the lattice study of πK scattering without properly understanding the contribution from the disconnected diagrams.

The recent years have seen a systematic development of a theory analysis of contraction diagrams in hadron-hadron interactions based on Partially-Quenched Chiral Perturbation Theory (PQChPT). The underlying principle is rather straightforward: Contraction diagrams that are inseparable in a physical amplitude would become separable upon the introduction of extra quark flavors. Since this separation is unphysical, it will unavoidably involve new parameters that cannot be fixed by experiment, but can be determined from lattice simulations. This method was successfully applied in the analysis of $\pi\pi$

---

[1]For investigations of πK scattering using dispersion relations, see e.g. [5, 6].
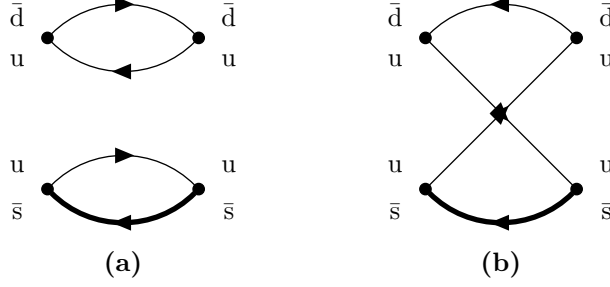
Figure 1: The quark contraction diagrams for $I = 3/2$ πK scattering. The amplitude for diagram **(a)** and **(b)** is given by $T_a(s,t,u)$ and $T_b(s,t,u)$ respectively. The thick line indicates the $\langle s\bar{s}\rangle$ contraction. The time flows in the horizontal direction.

scattering [24, 25, 26] and the parity-odd πN coupling [27]. In this paper we generalize it to πK scattering in both the finite and infinite volume. We demonstrate that, from the lattice calculation of the two easier computable connected diagrams in the $I = 3/2$ channel, one acquires enough information to make definite predictions of the exponential behavior of the harder to compute, disconnected diagram in $I = 1/2$. This provides a useful theory gauge to the calculation of the latter on lattice. For a discussion of the status of various scattering processes pertinent to chiral dynamics in the continuum and on the lattice, see [28].

This work is organized as follows. In Sec. 2 we introduce the different contraction diagrams in πK scattering, and demonstrate how they can be expressed in terms of physical scattering amplitudes in a deformation of QCD with an extended flavor sector. In Sec. 3 we introduce SU(4|1) PQChPT in the infinite volume, and use it to calculate the different contraction diagrams up to one-loop accuracy, $O(p^4)$. In Sec. 4 we discuss the implications of the results above to the actual lattice calculations which are carried out in a finite volume. The final conclusions are given in Sec. 5.

2. Contraction diagrams in πK scattering

Assuming isospin symmetry, the πK scattering amplitude can be categorized into two isospin channels, $T^{3/2}$ and $T^{1/2}$. In particular, $T^{3/2}(s,t,u)$ is given by the scattering amplitude of $\pi^+(k_1)K^+(p_1) \to \pi^+(k_2)K^+(p_2)$, where the Mandelstam variables s,t,u are defined as $s = (k_1 + p_1)^2$, $t = (k_1 - k_2)^2$, $u = (k_1 - p_2)^2$, respectively, subject to the constraint $s + t + u = 2(M_\pi^2 + M_K^2)$. The $I = 1/2$ amplitude can be obtained from $T^{3/2}$ by appropriate crossing:

$$T^{1/2}(s,t,u) = \frac{3}{2}T^{3/2}(u,t,s) - \frac{1}{2}T^{3/2}(s,t,u) \ . \tag{1}$$

To construct interpolators of mesons on the lattice, one expresses the meson fields in terms of their "constituent quarks", for example, $\pi^+ = u\bar{d}$ and $K^+ = u\bar{s}$. A lattice study of meson-meson scattering then consists of computing correlation functions involving all possible contractions between quark and anti-quark pairs. For instance, the $I = 3/2$ amplitude represents the sum of the two independent contraction diagrams $T_a(s,t,u)$ and $T_b(s,t,u)$ depicted in Fig. 1:

$$T^{3/2}(s,t,u) = T_a(s,t,u) + T_b(s,t,u). \tag{2}$$

Both contraction diagrams above are purely connected, as there is no contraction between the quark–anti-quark pair at the same time coordinate. Therefore, they are rather straightforwardly calculable on the lattice. The situation for the $I = 1/2$ amplitude is quite different. It involves three types of contraction diagrams displayed in Fig. 2:

$$T^{1/2}(s,t,u) = T_a(s,t,u) - \frac{1}{2}T_b(s,t,u) + \frac{3}{2}T_c(s,t,u) \ , \tag{3}$$
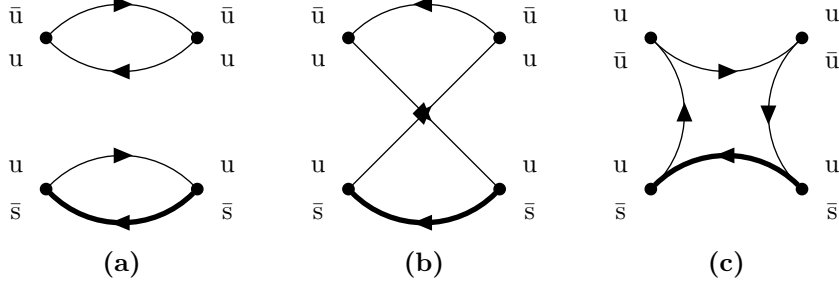
2

Figure 2: The contraction diagrams in the $I = 1/2$ πK scattering.

among which the diagram (c) contains a pair of disconnected contractions and is much noisier on the lattice. However, from the theory point of view, T_c is nothing but the $s \rightarrow u$ crossing of T_b and is no more complicated than the latter. Therefore, a precise theory description of the individual connected diagrams will automatically provide useful information of the disconnected ones which can be directly contrasted to lattice results.

In an ordinary three-flavor QCD the two connected diagrams in Fig. 1 are inseparable in any physical scattering amplitude, so one cannot study $T_b(s, t, u)$ by itself. The separation is possible, however, in a deformation of QCD with an extended quark sector. In a generic meson-meson scattering, in order to isolate each contraction diagram one requires a minimum number of four fermionic quarks [24]. But at the same time one needs also one "bosonic quark", such that its loop effect cancels with that from the extra fermionic quark, and thus to keep the sea dynamics identical to that of ordinary three-flavor QCD. This leads to SU(4|1) Partially-Quenched QCD (PQQCD), in which the quark sector reads $q = (u, d, s, j; \tilde{j})$, where the first four quarks are fermionic and the last is bosonic. The quark mass matrix is given by $\mathcal{M} = \text{diag}(\bar{m}, \bar{m}, m_s, \bar{m}; \bar{m})$, where m_s is the strange quark mass and $\bar{m} < m_s$. Notice that this extended theory is actually simpler than that needed in the analysis of $\pi\pi$ scattering [25, 26]. There, one needs again four fermionic quarks for the diagram separations, but two bosonic quarks in order to keep the sea dynamics identical to a two-flavor QCD. That leads to an SU(4|2) PQQCD which has more pseudo-Nambu-Goldstone (pNG) particles than SU(4|1) (see discussions in the next section). The two contractions T_a and T_b can now be expressed in terms of physical scattering amplitudes in the extended theory:

$$
\begin{aligned}
T_a(s, t, u) &= T_{(u\bar{s})(d\bar{j}) \rightarrow (u\bar{s})(d\bar{j})}(s, t, u) \ , \\
T_b(s, t, u) &= T_{(u\bar{s})(d\bar{j}) \rightarrow (d\bar{s})(u\bar{j})}(s, t, u) \ .
\end{aligned}
\tag{4}
$$

3. Analysis in SU(4|1) PQChPT

The right-hand side of Eq. (4) can be calculated in the low-energy effective field theory (EFT) of SU(4|1) PQQCD, namely the SU(4|1) PQChPT [29, 30, 31, 32, 33, 34, 35]. In this section we summarize the most important results relevant to this work, while interested readers may refer to the literature cited above for more details.

Firstly, in complete analogy to the ordinary ChPT, the spontaneous chiral symmetry breaking $\text{SU}(4|1)_L \otimes \text{SU}(4|1)_R \rightarrow \text{SU}(4|1)_V$ in SU(4|1) PQQCD generates pNG particles that are expressed collectively in the following matrix-valued field:

$$
\boldsymbol{\Phi} = \begin{pmatrix} \phi & \eta_1 \\ \eta_2 & \tilde{\phi} \end{pmatrix},
\tag{5}
$$

3

with:

$$\phi = \begin{pmatrix} u\bar{u} & u\bar{d} & u\bar{s} & u\bar{j} \\ d\bar{u} & d\bar{d} & d\bar{s} & d\bar{j} \\ s\bar{u} & s\bar{d} & s\bar{s} & s\bar{j} \\ j\bar{u} & j\bar{d} & j\bar{s} & j\bar{j} \end{pmatrix} , \quad \eta_1 = \begin{pmatrix} u\bar{\tilde{j}} \\ d\bar{\tilde{j}} \\ s\bar{\tilde{j}} \\ j\bar{\tilde{j}} \end{pmatrix} , \quad \eta_2 = \begin{pmatrix} \tilde{j}\bar{u} & \tilde{j}\bar{d} & \tilde{j}\bar{s} & \tilde{j}\bar{j} \end{pmatrix} , \quad \tilde{\phi} = \tilde{j}\bar{\tilde{j}} . \tag{6}$$

The supertrace (Str) of $\boldsymbol{\Phi}$ is defined as,

$$\mathrm{Str}\boldsymbol{\Phi} = \sum_{i=1}^{4} \phi_{ii} - \tilde{\phi}. \tag{7}$$

Since we know that there are only $5^2 - 1 = 24$ independent pNG particles in $\boldsymbol{\Phi}$ (in contrast to the $6^2 - 1 = 35$ pNG particles in SU(4|2) for $\pi\pi$ scattering), it is more convenient to introduce a supertraceless matrix $\boldsymbol{\Phi}' = \boldsymbol{\Phi} - \frac{1}{3}\mathrm{Str}\boldsymbol{\Phi}$. In particular, the diagonal components in $\boldsymbol{\Phi}'$ give rise to four independent neutral pNG bosons $\{\pi_0, \eta, \sigma_a, \sigma_b\}$ by writing:

$$(\boldsymbol{\Phi}')_{\mathrm{diag}} = \pi_0 \lambda_3' + \sigma_a \lambda_8' + \frac{1}{2\sqrt{2}}(3\eta - \sigma_b)\lambda_{15}' + \frac{1}{2\sqrt{2}}(-\eta + 3\sigma_b)\lambda_{24}' \tag{8}$$

where

$$\lambda_3' = \frac{1}{\sqrt{2}}\mathrm{diag}(1, -1, 0, 0; 0), \quad \lambda_8' = \frac{1}{\sqrt{6}}\mathrm{diag}(1, 1, 0, -2; 0),$$

$$\lambda_{15}' = \frac{1}{\sqrt{12}}\mathrm{diag}(1, 1, -3, 1; 0), \quad \lambda_{24}' = -\frac{1}{\sqrt{24}}\mathrm{diag}(1, 1, 1, 1; 4). \tag{9}$$

With this we can define the standard non-linear representation of the pNG particles,

$$U = \exp\left(\frac{\sqrt{2}i\boldsymbol{\Phi}'}{F_0}\right), \tag{10}$$

where F_0 is the pNG boson decay constant in the chiral limit, and proceed to construct the most general effective chiral Lagrangian. At O(p^2) we get:

$$\mathcal{L}^{(2)} = \frac{F_0^2}{4}\mathrm{Str}[\partial_\mu U^\dagger \partial^\mu U] + \frac{F_0^2}{4}\mathrm{Str}[\chi U^\dagger + U\chi^\dagger], \tag{11}$$

where $\chi = 2B_0\mathcal{M}$, with $\mathcal{M}$ the quark mass matrix. Expanding Eq. (11) up to the quadratic terms of pNG fields, we find that there are no mixing terms between different fields, and thus all the 24 pNG fields are indeed independent particles, with the leading order (LO) squared masses given by one of the three following mass parameters:

$$\mathring{M}_\pi^2 = 2B_0\bar{m}, \quad \mathring{M}_K^2 = B_0(\bar{m} + m_s), \quad \mathring{M}_\eta^2 = \frac{2}{3}B_0(\bar{m} + 2m_s), \tag{12}$$

satisfying the Gell-Mann-Okubo formula, $3\mathring{M}_\eta^2 = 4\mathring{M}_K^2 - \mathring{M}_\pi^2$. In particular, the four neutral particles $\{\pi_0, \eta, \sigma_a, \sigma_b\}$ have LO masses $\{\mathring{M}_\pi, \mathring{M}_\eta, \mathring{M}_\pi, \mathring{M}_\pi\}$, respectively. One also finds that the pNG field propagators are given by the standard form:

$$S_\phi(k) = \frac{i}{k^2 - M_\phi^2 + i\epsilon}, \tag{13}$$

except that the σ_b propagator acquires an extra negative sign. In short, the diagonalization procedure of the neutral particles in Eq.(8) completely avoids the cumbersome double-pole structures in the usual discussions of PQChPT propagators, and greatly simplifies the one-loop analysis.

4

Table 1: Coefficients of the UV divergence in the SU(4|1) PQChPT.

i	0	1	2	3	4	5	6	7	8
Γ_i	$\frac{1}{16}$	$\frac{3}{32}$	$\frac{3}{16}$	0	$\frac{1}{8}$	$\frac{3}{8}$	$\frac{11}{144}$	0	$\frac{5}{48}$

Applying the Lagrangian in Eq. (11) at one loop results in ultraviolet (UV) divergences that are regulated using dimensional regularization (DR) and reabsorbed into the LECs of the most general $O(p^4)$ chiral Lagrangian without external sources [34, 36]:

$$
\begin{aligned}
\mathcal{L}^{(4)} &= L_0 \text{Str}[(\partial_\mu U^\dagger)(\partial_\nu U)(\partial^\mu U^\dagger)(\partial^\nu U)] \\
&+ (L_1 - \frac{1}{2}L_0)\text{Str}[(\partial_\mu U^\dagger)(\partial^\mu U)]\text{Str}[(\partial_\nu U^\dagger)(\partial^\nu U)] \\
&+ (L_2 - L_0)\text{Str}[(\partial_\mu U^\dagger)(\partial_\nu U)]\text{Str}[(\partial^\mu U^\dagger)(\partial^\nu U)] \\
&+ (L_3 + 2L_0)\text{Str}[(\partial_\mu U^\dagger)(\partial^\mu U)(\partial_\nu U^\dagger)(\partial^\nu U)] \\
&+ L_4 \text{Str}[(\partial_\mu U^\dagger)(\partial^\mu U)]\text{Str}[U^\dagger\chi + \chi^\dagger U] \\
&+ L_5 \text{Str}[(\partial_\mu U^\dagger)(\partial^\mu U)(U^\dagger\chi + \chi^\dagger U)] \\
&+ L_6 (\text{Str}[U^\dagger\chi + \chi^\dagger U])^2 + L_7 (\text{Str}[U^\dagger\chi - \chi^\dagger U])^2 \\
&+ L_8 \text{Str}[\chi U^\dagger\chi U^\dagger + \chi^\dagger U\chi^\dagger U] \, .
\end{aligned}
\tag{14}
$$

Here it is useful to notice that the LECs $\{L_i\}_{i=1}^8$ are identical to those in the ordinary SU(3) ChPT [1], and the only new LEC is L_0. This can be seen by observing that Eq. (14) is equivalent to the $O(p^4)$ chiral Lagrangian of the ordinary SU(3) ChPT at tree level as long as the involved particles are the ordinary SU(3) pNG bosons. The renormalized LECs are defined by $L_i^r = L_i - \lambda\Gamma_i$, where

$$
\lambda = -\frac{1}{32\pi^2}\left(\frac{2}{4-d} + \log(4\pi) - \gamma_E + 1\right),
\tag{15}
$$

with γ_E the Euler-Mascheroni constant, and d is the number of space-time dimensions. The divergence (β-function) coefficients $\{\Gamma_i\}$ are summarized in Tab. 1.

Below we quote the analytical results up to $O(p^4)$ needed in this work. First, the physical pion, kaon masses and the pion decay constant are just the same as in ordinary ChPT [1]:

$$
\begin{aligned}
M_\pi^2 &= \mathring{M}_\pi^2\left[1 + \mu_\pi - \frac{\mu_\eta}{3} + \frac{16M_K^2}{F_\pi^2}(2L_6^r - L_4^r) + \frac{8M_\pi^2}{F_\pi^2}(2L_6^r + 2L_8^r - L_4^r - L_5^r)\right], \\
M_K^2 &= \mathring{M}_K^2\left[1 + \frac{2\mu_\eta}{3} + \frac{8M_\pi^2}{F_\pi^2}(2L_6^r - L_4^r) + \frac{8M_K^2}{F_\pi^2}(4L_6^r + 2L_8^r - L_4^r - L_5^r)\right], \\
F_\pi &= F_0\left[1 - 2\mu_\pi - \mu_K + \frac{8M_K^2}{F_\pi^2}L_4^r + \frac{4M_\pi^2}{F_\pi^2}(L_4^r + L_5^r)\right],
\end{aligned}
\tag{16}
$$

where $\mu_P = (M_P^2/32\pi^2 F_\pi^2)\ln(M_P^2/\mu^2)$, with μ the scale of dimensional regularization.

The two contraction diagrams T_a and T_b, expressed as SU(4|1) physical scattering amplitudes in Eq. (4), are given up to $O(p^4)$ as:

$$
\begin{aligned}
T_a(s,t,u) &= \frac{\mu_\pi}{8F_\pi^2 M_\pi^2(M_\pi^2 - M_K^2)}[16M_K^4 M_\pi^2 + 2M_K^2(14M_\pi^4 - 7M_\pi^2 t + t^2) \\
&+ M_\pi^2(16M_\pi^4 - 15M_\pi^2 t - 6s^2 - 4su - 6u^2)] + \frac{\mu_K}{4F_\pi^2 M_K^2(M_K^2 - M_\pi^2)} \\
&[8M_K^6 + 8M_K^4(2M_\pi^2 - t) + M_K^2(8M_\pi^4 - 8M_\pi^2 t - 3s^2 - 2su - 3u^2)
\end{aligned}
$$

5

$$+M_\pi^2 t^2] + \frac{M_\pi^2 \mu_\eta}{72 F_\pi^2 M_\eta^2 (M_K^2 - M_\pi^2)} [-32 M_K^4 + M_K^2 (18t - 4M_\pi^2)$$

$$+9M_\pi^2 t] + \frac{t(M_\pi^2 + t)}{8F_\pi^4} \bar{J}_{\pi\pi}(t) - \frac{M_\pi^2 (8M_K^2 - 9t)}{72 F_\pi^4} \bar{J}_{\eta\eta}(t) + \frac{t^2}{8F_\pi^4} \bar{J}_{KK}(t)$$

$$+\frac{(M_K^2 + M_\pi^2 - s)^2}{4F_\pi^4} \bar{J}_{\pi K}(s) + \frac{(M_K^2 + M_\pi^2 - u)^2}{4F_\pi^4} \bar{J}_{\pi K}(u)$$

$$+\frac{M_\pi^2 (4M_K^2 - 3t)}{12 F_\pi^4} \bar{J}_{\pi\eta}(t) + \frac{8}{F_\pi^4} [3M_K^4 + M_K^2 (4M_\pi^2 - 2t)$$

$$+3M_\pi^4 - 2M_\pi^2 t - s^2 - su - u^2] L_0^r + \frac{8}{F_\pi^4} (t - 2M_K^2)(t - 2M_\pi^2) L_1^r$$

$$+\frac{4}{F_\pi^4} [(s - M_\pi^2 - M_K^2)^2 + (u - M_\pi^2 - M_K^2)^2] L_2^r + \frac{8}{F_\pi^4} [M_K^2 (t - 4M_\pi^2)$$

$$+M_\pi^2 t] L_4^r + \frac{32 M_K^2 M_\pi^2}{F_\pi^4} L_6^r + \frac{4M_K^2 M_\pi^2 - 9t(M_\pi^2 + t)}{576 \pi^2 F_\pi^4} \tag{17}$$

and

$$T_b(s,t,u) \;=\; \frac{M_K^2 + M_\pi^2 - s}{2F_\pi^2} + \frac{\mu_\pi}{24 F_\pi^2 M_\pi^2 (M_\pi^2 - M_K^2)} [-2M_K^4 (9M_\pi^2 + 2t)$$

$$+M_K^2 (6M_\pi^4 + 3M_\pi^2 (5t + 6u) + 8t^2 + 4tu) + M_\pi^2 (24 M_\pi^4 - 2M_\pi^2$$

$$(4t + 9u) - 8t^2 - 7tu - 6u^2)] + \frac{\mu_K}{12 F_\pi^2 M_K^2 (M_K^2 - M_\pi^2)} [30 M_K^6$$

$$+2M_K^4 (9M_\pi^2 - 10t - 12u) + M_K^2 (3M_\pi^2 (3t - 4u) - 2t^2 + 2tu + 6u^2)$$

$$+M_\pi^2 t (-M_\pi^2 + 2t + u)] + \frac{\mu_\eta}{8F_\pi^2 (M_K^2 - M_\pi^2)} [-18 M_K^4 + M_K^2 (15t$$

$$+18u - 10 M_\pi^2) - 6M_\pi^2 (t - u) - 3tu - 6u^2] + \frac{1}{12 F_\pi^4} [2t^2 + tu + 4M_\pi^4$$

$$+M_K^2 (4M_\pi^2 - t) - 2M_\pi^2 (3t + 2u)] \bar{J}_{\pi\pi}(t)$$

$$+\frac{1}{24 F_\pi^4} [4M_K^4 + M_K^2 (4M_\pi^2 - 3t - 4u) + t(-M_\pi^2 + 2t + u)] \bar{J}_{KK}(t)$$

$$+\frac{1}{16 F_\pi^4} [-4M_K^4 + M_K^2 (8M_\pi^2 - 2t) - 4M_\pi^4 - 2M_\pi^2 t + tu + 2u^2] \bar{J}_{\pi K}(u)$$

$$+\frac{t}{16 F_\pi^4} \frac{(M_K^2 - M_\pi^2)^2}{u} \bar{J}_{\pi K}(u) - \frac{M_\pi^2 (4M_K^2 - 3t)}{12 F_\pi^4} \bar{J}_{\pi\eta}(t) + \frac{1}{144 F_\pi^4} [44 M_K^4$$

$$+M_K^2 (56 M_\pi^2 - 42t - 48u) - 4M_\pi^4 + 6M_\pi^2 (t - 4u) + 9tu + 18u^2] \bar{J}_{K\eta}(u)$$

$$-\frac{(M_K^2 - M_\pi^2)^2 (16 M_K^2 - 8M_\pi^2 - t)}{144 F_\pi^4} \frac{\bar{J}_{K\eta}(u)}{u} + \frac{(M_K^2 - M_\pi^2)^4}{72 F_\pi^4 u^2} (9 \bar{\bar{J}}_{\pi K}(u) + \bar{\bar{J}}_{K\eta}(u))$$

$$-\frac{8}{F_\pi^4} [-s^2 - su - u^2 + 3M_K^4 + M_K^2 (4M_\pi^2 - 2t) + 3M_\pi^4 - 2M_\pi^2 t] L_0^r + \frac{2}{F_\pi^4} [(t - 2M_K^2)$$

$$(t - 2M_\pi^2) + (u - M_\pi^2 - M_K^2)^2] L_3^r - \frac{4M_\pi^2 (M_K^2 - M_\pi^2 + s)}{F_\pi^4} L_5^r$$

$$+\frac{16 M_K^2 M_\pi^2}{F_\pi^4} L_8^r + \frac{1}{384 \pi^2 F_\pi^4} [11 M_K^4 + M_K^2 (10 M_\pi^2 - 9t - 7u) + 3M_\pi^4$$

$$+M_\pi^2 (5t - 3u) - 5t^2 + tu + u^2] \,. \tag{18}$$

Here, the two-point functions $\bar{J}_{PQ}$ and $\bar{\bar{J}}_{PQ}$ are defined as [37]:

$$\bar{J}_{PQ}(s) = \frac{1}{32\pi^2}\left[2+\left(\frac{\Delta}{s}-\frac{\Sigma}{\Delta}\right)\ln\frac{M_Q^2}{M_P^2}-\frac{\nu(s)}{s}\ln\frac{[s+\nu(s)]^2-\Delta^2}{[s-\nu(s)]^2-\Delta^2}\right]$$

$$\bar{\bar{J}}_{PQ}(s) = \bar{J}_{PQ}(s)-\frac{s}{32\pi^2}\left[\frac{\Sigma}{\Delta^2}+2\frac{M_P^2 M_Q^2}{\Delta^3}\ln\frac{M_Q^2}{M_P^2}\right], \tag{19}$$

where
$$\Delta = M_P^2 - M_Q^2, \ \ \Sigma = M_P^2 + M_Q^2, \ \ \nu(s)=\sqrt{[s-(M_P+M_Q)^2][s-(M_P-M_Q)^2]}. \tag{20}$$

The third contraction diagram is simply given by $T_c(s,t,u) = T_b(u,t,s)$. Finally, we are also interested in their values at the threshold, $s_0 = (M_K + M_\pi)^2$, $t_0 = 0$ and $u_0 = (M_K - M_\pi)^2$, which are given by:

$$(T_a)_{\text{thr}} = \frac{M_K^2 M_\pi^2}{F_\pi^2(M_K^2-M_\pi^2)}\left(\frac{9}{2}\mu_\pi-4\mu_K-\frac{8M_K^2+M_\pi^2}{18M_\eta^2}\mu_\eta\right)+\frac{M_K^2 M_\pi^2}{F_\pi^4}(-48L_0^r+32L_1^r$$

$$+32L_2^r-32L_4^r+32L_6^r+\bar{J}_{\pi K}(s_0)+\bar{J}_{\pi K}(u_0))+\frac{M_K^2 M_\pi^2}{144\pi^2 F_\pi^4} \tag{21}$$

$$(T_b)_{\text{thr}} = -\frac{M_K M_\pi}{F_\pi^2}+\frac{\mu_\pi}{4F_\pi^2(M_K^2-M_\pi^2)}[M_K^4+2M_K^3 M_\pi+5M_K^2 M_\pi^2-10M_K M_\pi^3]$$

$$+\frac{\mu_K}{2F_\pi^2(M_K-M_\pi)}[2M_K^3+2M_K^2 M_\pi+M_K M_\pi^2-M_\pi^3]$$

$$-\frac{\mu_\eta}{4F_\pi^2(M_K^2-M_\pi^2)}[3M_K^4+6M_K^3 M_\pi+11M_K^2 M_\pi^2-6M_K M_\pi^3]$$

$$-\frac{1}{8F_\pi^4}[(M_K-M_\pi)^2(M_K^2+6M_K M_\pi+M_\pi^2)]\bar{J}_{\pi K}(u_0)-\frac{1}{72F_\pi^4}[M_K^4$$

$$+4M_K^3 M_\pi-42M_K^2 M_\pi^2+4M_K M_\pi^3+M_\pi^4]\bar{J}_{K\eta}(u_0)+\frac{(M_K+M_\pi)^4}{72F_\pi^4}(9\bar{\bar{J}}_{\pi K}(u_0)$$

$$+\bar{\bar{J}}_{K\eta}(u_0))+\frac{8M_K^2 M_\pi^2}{F_\pi^4}\left(6L_0^r+2L_3^r-\frac{M_K+M_\pi}{M_K}L_5^r+2L_8^r\right)$$

$$+\frac{(M_K+M_\pi)^2(5M_K^2+M_\pi^2)}{384\pi^2 F_\pi^4} \tag{22}$$

and $(T_c)_{\text{thr}}$ is obtained by replacing $M_\pi \to -M_\pi$ (which also means $u_0 \to s_0$) in $(T_b)_{\text{thr}}$.

4. Finite-Volume Analysis

We now discuss the implications of the results above, which are obtained in a field theory at infinite volume, to the discrete energies calculated on the lattice in a finite volume. The analysis in this section is a straightforward generalization of that in Ref. [26].

To do so we construct three effective single-channel scattering amplitudes using T_a, T_b and T_c. First, consider the 2×2 scattering matrix between the asymptotic states $|\psi_1\rangle = |u\bar{s}\rangle |d\bar{j}\rangle$ and $|\psi_2\rangle = |d\bar{s}\rangle |u\bar{j}\rangle$. Diagonalizing this matrix gives two single-channel scattering amplitudes:

$$T_\alpha(s,t,u) = T_a(s,t,u)+T_b(s,t,u), \ \ T_\beta(s,t,u) = T_a(s,t,u)-T_b(s,t,u). \tag{23}$$

In particular, $T_\alpha(s,t,u) = T^{3/2}(s,t,u)$. The third single-channel amplitude is simply:

$$T_\gamma(s,t,u) = T^{1/2}(s,t,u) = T_a(s,t,u)-\frac{1}{2}T_b(s,t,u)+\frac{3}{2}T_c(s,t,u). \tag{24}$$

7

For each single-channel amplitude one could perform the partial-wave expansion in the center-of-mass (CM) frame:

$$T(s,t,u) = \sum_{l=0}^{\infty} (2l+1)T_l(E)P_l(\cos\theta),$$ (25)

where $E = \sqrt{s}$ is the CM energy, θ is the scattering angle and $\{P_l(x)\}$ are the Legendre polynomials. The $l = 0$ (i.e. S-wave) partial-wave amplitude is parameterized as:

$$T_0(E) = \frac{8\pi E}{p\cot\delta_0(E) - ip},$$ (26)

where p is the CM momentum and $\delta_0(E)$ is the S-wave phase shift. At small p one performs the effective range expansion:

$$p\cot\delta_0(E) = -\frac{1}{a_0} + \frac{1}{2}r_0 p^2 + \dots ,$$ (27)

which defines the S-wave scattering length a_0 and effective range r_0. The S-wave scattering lengths of the three single-channel amplitudes above are given by:

$$
\begin{aligned}
a_0^\alpha &= -\frac{1}{8\pi\sqrt{s_0}}\left[(T_a)_{\text{thr}} + (T_b)_{\text{thr}}\right] , \\
a_0^\beta &= -\frac{1}{8\pi\sqrt{s_0}}\left[(T_a)_{\text{thr}} - (T_b)_{\text{thr}}\right] , \\
a_0^\gamma &= -\frac{1}{8\pi\sqrt{s_0}}\left[(T_a)_{\text{thr}} - \frac{1}{2}(T_b)_{\text{thr}} + \frac{3}{2}(T_c)_{\text{thr}}\right] .
\end{aligned}
$$ (28)

In particular, a_0^β is the only one among the three that depends on the unphysical LEC L_0^r. The latter does not affect the pNG boson masses and decay constants at $\mathcal{O}(p^4)$, but does contribute to the scattering parameters.

The discrete energies E extracted from lattice correlation functions at finite volume can be obtained by solving the single-channel Lüscher's formula [38] (see also Ref. [20, 39] for more discussions):

$$p\cot\delta_0(E) = \frac{2\pi}{L}\pi^{-3/2}\mathcal{Z}_{00}(1;q^2), \quad q = p\frac{L}{2\pi},$$ (29)

where L is the lattice size and $\mathcal{Z}_{00}$ is the Lüscher zeta-function. This gives the discrete ground-state energies of the three channels as known functions of the scattering lengths and lattice size $E_0^i = f(a_0^i, L)$, $(i = \alpha, \beta, \gamma)$. Therefore, if we define $C_i(\tau)$ $(i = a, b, c)$ as the lattice correlation function corresponding to the contraction diagram of type i at the Euclidean time τ, then the following combinations of correlation functions decay as a single exponential at large τ:

$$
\begin{aligned}
C_a(\tau) + C_b(\tau) &\sim A_\alpha \exp\{-E_0^\alpha \tau\} , \\
C_a(\tau) - C_b(\tau) &\sim A_\beta \exp\{-E_0^\beta \tau\} , \\
C_a(\tau) - \frac{1}{2}C_b(\tau) + \frac{3}{2}C_c(\tau) &\sim A_\gamma \exp\{-E_0^\gamma \tau\} .
\end{aligned}
$$ (30)

Hence, through a single lattice calculation of the difference between C_a and C_b which both appear in the $I = 3/2$ channel, one is able to obtain E_0^β and thus fix the unknown LEC L_0^r. After doing so, all the three discrete energies $\{E_0^\alpha, E_0^\beta, E_0^\gamma\}$ are fully predictable given any set of lattice parameters. This is beneficial in multiple ways. For instance, we know that the most difficult disconnected correlation function $C_c(\tau)$ depends on three exponents:

$$C_c(\tau) \sim -\frac{1}{6}A_\alpha \exp\{-E_0^\alpha \tau\} - \frac{1}{2}A_\beta \exp\{-E_0^\beta \tau\} + \frac{2}{3}A_\gamma \exp\{-E_0^\gamma \tau\} ,$$ (31)

and all the three exponents are known functions of $\{\bar{m}, m_s, L\}$. This provides a useful theory gauge of the accuracy for lattice studies of $C_c(\tau)$, which directly tests the lattice techniques in handling disconnected diagrams. Furthermore, once L_0^r is fixed from lattice data, the SU(4|1) chiral Lagrangian (without external sources) will be completely known to NLO, so it could be applied to the lattice study of other interesting hadronic processes such as the $\pi\pi \to K\bar{K}$ scattering.

We end this section by estimating the LEC L_0^r. Integrating out the strange quark from the theory, the graded algebra SU(4|1) reduces to SU(3|1). The LEC L_0 appearing in this reduced theory should be the same as in the SU(4|2) version and thus is known with a sizeable uncertainty, $L_0^r = 1.1(1.0) \cdot 10^{-3}$, which comes from an NNLO analysis of lattice data in Ref. [40]. In our new formalism, L_0^r appears at NLO in the SU(4|1) scattering amplitudes, so one could in general expect an order-of-magnitude improvement of its accuracy through the analysis of the lattice πK contraction diagrams, just like what happened to the combination $3L_0^r + L_3^r$ in SU(4|2) as demonstrated in Ref. [26]. The actual analysis will appear in a future work.

5. Conclusions

As a natural generalization of previous works, we perform a PQChPT analysis of the different contraction diagrams in πK scattering, in both infinite and finite volume. We show that up to $\mathcal{O}(p^4)$ there is only one undetermined LEC in the EFT, which can be fixed by the lattice study of the connected contraction diagrams in the $I = 3/2$ channel. After doing so, the large-τ behavior of the disconnected correlation function in the $I = 1/2$ channel is predictable as a function of lattice parameters. These theory predictions can then be contrasted with actual lattice calculations, serving as an important cross-check to the latter and reducing their associated systematic uncertainties. Finally, the theory analysis above can be generalized to πN scattering and will be carried out in a follow-up work.

References

[1] J. Gasser and H. Leutwyler, Nucl. Phys. B **250**, 465 (1985).

[2] V. Bernard, N. Kaiser and U.-G. Meißner, Nucl. Phys. B **357**, 129 (1991).

[3] V. Bernard, N. Kaiser and U.-G. Meißner, Phys. Rev. D **43**, 2757 (1991).

[4] J. Bijnens, P. Dhonte and P. Talavera, JHEP **0405**, 036 (2004) [hep-ph/0404150].

[5] P. Buettiker, S. Descotes-Genon and B. Moussallam, Eur. Phys. J. C **33**, 409 (2004) [hep-ph/0310283].

[6] J. R. Pelaez, A. Rodas and J. Ruiz de Elvira, Eur. Phys. J. C **77**, no. 2, 91 (2017) [arXiv:1612.07966 [hep-ph]].

[7] G. S. Bali *et al.* [RQCD Collaboration], Phys. Rev. D **93**, no. 9, 094504 (2016) [arXiv:1603.00827 [hep-lat]].

[8] Y. B. Yang *et al.* [xQCD Collaboration], Phys. Rev. D **94**, no. 5, 054503 (2016) [arXiv:1511.09089 [hep-lat]].

[9] A. Abdel-Rehim *et al.* [ETM Collaboration], Phys. Rev. Lett. **116**, no. 25, 252001 (2016) [arXiv:1601.01624 [hep-lat]].

[10] N. Yamanaka *et al.* [JLQCD Collaboration], Phys. Rev. D **98**, no. 5, 054516 (2018) [arXiv:1805.10507 [hep-lat]].

[11] S. Durr *et al.*, Phys. Rev. Lett. **116**, no. 17, 172001 (2016) [arXiv:1510.08013 [hep-lat]].

[12] M. Hoferichter, J. Ruiz de Elvira, B. Kubis and U.-G. Meißner, Phys. Rev. Lett. **115**, 092301 (2015) [arXiv:1506.04142 [hep-ph]].

[13] M. Hoferichter, J. Ruiz de Elvira, B. Kubis and U.-G. Meißner, Phys. Rev. Lett. **115**, no. 19, 192301 (2015) [arXiv:1507.07552 [nucl-th]].

[14] M. Hoferichter, J. Ruiz de Elvira, B. Kubis and U.-G. Meißner, Phys. Lett. B **760**, 74 (2016) [arXiv:1602.07688 [hep-lat]].

[15] J. Ruiz de Elvira, M. Hoferichter, B. Kubis and U.-G. Meißner, J. Phys. G **45**, no. 2, 024001 (2018) [arXiv:1706.01465 [hep-ph]].

[16] C. Miao, X. i. Du, G. w. Meng and C. Liu, Phys. Lett. B **595**, 400 (2004) [hep-lat/0403028].

[17] S. R. Beane, P. F. Bedaque, T. C. Luu, K. Orginos, E. Pallante, A. Parreno and M. J. Savage, Phys. Rev. D **74**, 114503 (2006) [hep-lat/0607036].

[18] J. Nagata, S. Muroya and A. Nakamura, Phys. Rev. C **80**, 045203 (2009) Erratum: [Phys. Rev. C **84**, 019904 (2011)] [arXiv:0812.1753 [hep-lat]].

[19] Z. Fu, Phys. Rev. D **85**, 074501 (2012) [arXiv:1110.1422 [hep-lat]].

[20] C. B. Lang, L. Leskovec, D. Mohler and S. Prelovsek, Phys. Rev. D **86**, 054508 (2012) [arXiv:1207.3204 [hep-lat]].

[21] K. Sasaki *et al.* [PACS-CS Collaboration], Phys. Rev. D **89**, no. 5, 054502 (2014) [arXiv:1311.7226 [hep-lat]].

[22] D. J. Wilson, J. J. Dudek, R. G. Edwards and C. E. Thomas, Phys. Rev. D **91**, no. 5, 054008 (2015) [arXiv:1411.2004 [hep-ph]].

[23] C. Helmes *et al.* [ETM Collaboration], Phys. Rev. D **98**, no. 11, 114511 (2018) [arXiv:1809.08886 [hep-lat]].

[24] F. K. Guo, L. Liu, U.-G. Meißner and P. Wang, Phys. Rev. D **88**, 074506 (2013) [arXiv:1308.2545 [hep-lat]].

[25] N. R. Acharya, F. K. Guo, U.-G. Meißner and C. Y. Seng, Nucl. Phys. B **922**, 480 (2017) [arXiv:1704.06754 [hep-lat]].

[26] N. R. Acharya, F. K. Guo, U.-G. Meißner and C. Y. Seng, JHEP **1904**, 165 (2019) [arXiv:1902.10290 [hep-lat]].

[27] F. K. Guo and C. Y. Seng, Eur. Phys. J. C **79**, no. 1, 22 (2019) [arXiv:1809.00639 [nucl-th]].

[28] U.-G. Meißner, PoS CD **2018**, 013 (2018) [arXiv:1903.02898 [hep-ph]].

[29] C. W. Bernard and M. F. L. Golterman, Phys. Rev. D **49**, 486 (1994) [hep-lat/9306005].

[30] S. R. Sharpe and N. Shoresh, Nucl. Phys. Proc. Suppl. **83**, 968 (2000) [hep-lat/9909090].

[31] S. R. Sharpe and N. Shoresh, Phys. Rev. D **62**, 094503 (2000) [hep-lat/0006017].

[32] S. R. Sharpe and N. Shoresh, Phys. Rev. D **64**, 114510 (2001) [hep-lat/0108003].

[33] C. Bernard and M. Golterman, Phys. Rev. D **88**, no. 1, 014004 (2013) [arXiv:1304.1948 [hep-lat]].

[34] S. R. Sharpe, hep-lat/0607016.

[35] M. Golterman, arXiv:0912.4042 [hep-lat].

[36] L. Giusti and M. Lüscher, JHEP **0903**, 013 (2009) [arXiv:0812.3638 [hep-lat]].

[37] A. Gomez Nicola and J. R. Pelaez, Phys. Rev. D **65**, 054009 (2002) [hep-ph/0109056].

[38] M. Lüscher, Commun. Math. Phys. **105**, 153 (1986).

[39] M. Döring, U.-G. Meißner, E. Oset and A. Rusetsky, Eur. Phys. J. A **47**, 139 (2011) [arXiv:1107.3988 [hep-lat]].

[40] P. Boyle, N. Christ, N. Garron, C. Jung, A. Jttner, C. Kelly, R. Mawhinney, G. McGlynn, D. Murphy, S. Ohta, A. Portelli and C. Sachrajda, Phys. Rev. D **93** (2016) no.5, 054502 [arXiv:1511.01950 [hep-lat]].